J. Fluid Mech. (1977), *vol.* 80, *part* 1, *pp.* 99–128
Printed in Great Britain

Prediction of the contributions to the Reynolds stress from bursting events in open-channel flows

By HIROJI NAKAGAWA AND IEHISA NEZU
Department of Civil Engineering, Kyoto University, Kyoto 606, Japan

(Received 9 October 1975 and in revised form 1 June 1976)

In this paper we intend to predict the magnitude of the contribution to the Reynolds stress of bursting events: 'ejections', 'sweeps', 'inward interactions' and 'outward interactions'. We shall do this by making use of the conditional probability distribution of the Reynolds stress $-uv$, which can be derived by applying the cumulant-discard method to the Gram–Charlier probability distribution of the two variables u and v. The Reynolds-stress fluctuations in open-channel flows over smooth and rough beds are measured by dual-sensor hot-film anemometers, whose signals are conditionally sampled and sorted into the four quadrants of the u, v plane by using a high-speed digital data processing system.

We shall verify that even the third-order conditional probability distribution of the Reynolds stress shows fairly good agreement with the experimental results and that the sequence of events in the bursting process, i.e. ejections, sweeps and interactions, is directly related to the turbulent energy budget in the form of turbulent diffusion. Also, we shall show that the roughness effect is marked in the area from the wall to the middle of the equilibrium region, and that sweeps appear to be more important than ejections as the roughness increases and as the distance from the wall decreases.

1. Introduction

Intensive research on the dynamics of wall turbulence in air flow has been performed by many investigators in the last twenty years. On the other hand, turbulence measurements in water flow were begun only about eight years ago with the development of hot-film anemometers. We (Nakagawa, Nezu & Ueda 1975) recently published a report on turbulence measurements in open-channel flow and clarified the fine-structure of turbulence from the viewpoint of the turbulent energy budget.

The physics of turbulence have now been established in at least a qualitative sense through experiments and refined data analysis, as pointed out by Mollo-Christensen (1971). Kline *et al.* (1967) and Kim, Kline & Reynolds (1971) discovered the bursting phenomenon, in which ejections played a predominant role, by making visual studies of the mechanism of turbulence production by the hydrogen-bubble technique. Also, Corino & Brodkey (1969) and Grass (1971) found by flow visualization that sweeps are prominent near the wall. This suggests

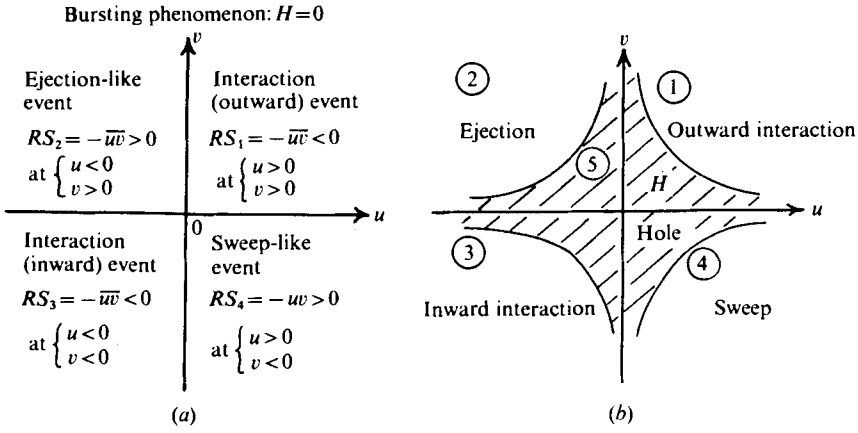

FIGURE 1. Schematic division of the bursting phenomenon.

that sweeps may be as important as ejections for turbulence production. This was verified by Nychas, Hershey & Brodkey (1973) and Offen & Kline (1974).

On the basis of these qualitative results, some researchers have attempted to obtain more quantitative knowledge about the structure of the Reynolds stress, i.e. turbulence production, by using point measurements. Such studies have been made by Frenkiel & Klebanoff (1967), who used an improved digital method of analysis, and by Kovasznay, Kibens & Blackwelder (1970), who used the conditional sampling method. Wallace, Eckelmann & Brodkey (1972) and Brodkey, Wallace & Eckelmann (1974) measured velocity fluctuations near the wall in oil flow by using an X-probe. They then divided the plane of the streamwise and normal fluctuating velocity components u and v into four quadrants, as shown in figure 1, in order to evaluate the contributions of the ejections and sweeps to the Reynolds stress. As pointed out by Brodkey *et al.* (1974), it seems appropriate to provide unifying terminology for the names of the events. Here, 'ejection' ($u < 0$, $v > 0$), 'sweep' ($u > 0$, $v < 0$), 'inward interaction' ($u < 0$, $v < 0$) and 'outward interaction' ($u > 0$, $v > 0$) are used systematically.

Willmarth & Lu (1972) and Lu & Willmarth (1973) also analysed the Reynolds-stress fluctuations in a turbulent boundary layer by using the conditional sampling method; they obtained nearly the same results as Wallace *et al.* (1972) except very close to the wall.

Wallace *et al.* (1972), Willmarth & Lu (1972), Gupta & Kaplan (1972), Antonia & Atkinson (1973) and others investigated the statistical characteristics of the Reynolds stress, paying attention to its intermittency, but none of them could obtain a definite relationship for the magnitude of each event or its physical interpretation because they did not take account of its conditional probability density distribution. It is very remarkable that Brodkey *et al.* (1974) measured the conditional probability distributions of u, v and uv and described their characteristics but could not obtain these distribution functions theoretically.

In the light of the above, this paper will show that the conditional probability distribution of the Reynolds stress may be introduced theoretically by making

use of the cumulant expansion method for the two variables u and v, in order to predict the magnitude of the contribution to the Reynolds stress from each event.

2. Theoretical considerations

In this section we are going to evaluate the contribution of the bursting events to the Reynolds stress by theoretical analysis. To begin with, we normalize the velocity fluctuations by dividing by the turbulence intensity in each direction (r.m.s. value) so that $\hat{u} \equiv u/u'$ and $\hat{v} \equiv v/v'$, where $u' \equiv (\overline{u^2})^{\frac{1}{2}}$ and $v' \equiv (\overline{v^2})^{\frac{1}{2}}$. Denoting the joint probability function of $\hat{u}$ and $\hat{v}$ by $p(\hat{u}, \hat{v})$, its characteristic function by $\Phi(\xi, \eta)$, the moment of $\overline{\hat{u}^j \hat{v}^k}$ by M_{jk} and the corresponding cumulant by Q_{jk}, the following definitions can be given as indicated by Monin & Yaglom (1971):

$$\Phi(\xi, \eta) = \iint_{-\infty}^{\infty} \exp\{i(\hat{u}\xi + \hat{v}\eta)\} p(\hat{u}, \hat{v})\, d\hat{u}\, d\hat{v}, \tag{1}$$

$$M_{jk} = \frac{1}{i^{j+k}} \frac{\partial^{j+k}}{\partial \xi^j \partial \eta^k} \Phi(\xi, \eta)|_{\xi=\eta=0}, \tag{2}$$

$$Q_{jk} = \frac{1}{i^{j+k}} \frac{\partial^{j+k}}{\partial \xi^j \partial \eta^k} \ln \Phi(\xi, \eta)|_{\xi=\eta=0}. \tag{3}$$

Here, $\Phi(\xi, \eta)$ is the Fourier transform of $p(\hat{u}, \hat{v})$, and ξ and η are its arguments. Expanding $\Phi(\xi, \eta)$ in a Taylor series about $\xi = \eta = 0$ yields

$$\Phi(\xi, \eta) = \sum_{n=0}^{\infty} \frac{1}{n!} \left(\xi \frac{\partial}{\partial \xi'} + \eta \frac{\partial}{\partial \eta'}\right)^n \Phi(\xi', \eta')|_{\xi'=\eta'=0}. \tag{4}$$

Thus M_{jk} and Q_{jk} correspond to the coefficients in Taylor expansions of $\Phi(\xi, \eta)$ and $\ln \Phi(\xi, \eta)$ respectively. The relations between the moments and the cumulants are successively obtained by making use of (2), (3) and (4).

Now, since $M_{10} = \overline{\hat{u}} = 0$, $M_{01} = \overline{\hat{v}} = 0$, $M_{20} = \overline{\hat{v}^2} = 1$, $M_{02} = \overline{\hat{v}^2} = 1$ and $M_{11} = \overline{\hat{u}\hat{v}} = \overline{u'v'} = -R < 0$ (correlation coefficient), the following can be obtained:

$$\left.\begin{aligned} Q_{00} = 1, \quad Q_{10} = 0, \quad Q_{20} = 1, \quad Q_{11} = -R, \quad Q_{30} = M_{30}, \quad Q_{21} = M_{21}, \\ Q_{40} = M_{40} - 3, \quad Q_{31} = M_{31} + 3R, \quad Q_{22} = M_{22} - 2R^2 - 1, \ldots. \end{aligned}\right\} \tag{5}$$

Q_{jk} for $j < k$ can be obtained by merely exchanging j and k in the terms of Q_{jk} for $j \geqslant k$.

In turbulent phenomena the cumulants of extremely high order can usually be neglected, and even in the theory of isotropic turbulence the fourth-order cumulant terms are sometimes discarded, e.g. by Rotta (1972). This suggests that approximation by the lower-order cumulants may be valid for phenomena mainly depending upon lower-order moments, because a cumulant is considered to be a measure of the deviation from a Gaussian distribution.

Taking into account the cumulants of less than fourth order, the following Taylor series can be obtained from (3) and (5):

$$\ln \Phi(\xi, \eta) = -\tfrac{1}{2}(\xi^2 - 2R\xi\eta + \eta^2) + \sum_{j+k=3}^{4} i^{j+k} \frac{Q_{jk}}{j!\,k!} \xi^j \eta^k. \tag{6}$$

Through an inverse transformation of (1) in which the terms of $\Phi(\xi, \eta)$ of less than fourth order are taken into account, $p(\hat{u}, \hat{v})$ can be written as

$$p(\hat{u}, \hat{v}) = \frac{1}{2\pi}\int\int_{-\infty}^{\infty} \Phi(\xi, \eta)\, e^{-i(\hat{u}\xi+\hat{v}\eta)}\, d\xi\, d\eta$$

$$= G(\hat{u}, \hat{v}) + \sum_{j+k=3}^{4} (-1)^{j+k} \frac{Q_{jk}}{j!\,k!} \frac{\partial^{j+k} G(\hat{u}, \hat{v})}{\partial \hat{u}^j \partial \hat{v}^k} \tag{7}$$

$$\equiv G(\hat{u}, \hat{v}) \left[1 + \sum_{j+k=3}^{4} \frac{Q_{jk}}{j!\,k!} H_{jk}(\hat{u}, \hat{v})\right], \tag{7a}$$

where $G(\hat{u}, \hat{v})$ is the Gaussian distribution for two variables, defined as

$$G(\hat{u}, \hat{v}) \equiv \frac{1}{2\pi(1-R^2)^{\frac{1}{2}}} \exp\left\{-\frac{\hat{u}^2 + 2R\hat{u}\hat{v} + \hat{v}^2}{2(1-R^2)}\right\}, \tag{8}$$

and $H_{jk}(\hat{u}, \hat{v})$ is a Hermite polynomial in two variables.

Equation (7*a*) represents a special form of joint probability density distribution of the Gram–Charlier type. According to Frenkiel & Klebanoff (1973), the generalized Gram–Charlier distribution in the following form extended by Kampé de Fériet (1966) should be used when higher-order terms are needed:

$$p(\hat{u}, \hat{v}) = G(\hat{u}, \hat{v}) \sum_{j+k=0}^{\infty} \frac{1}{j!\,k!} \overline{\tilde{H}_{jk}(\hat{u}, \hat{v})}\, H_{jk}(\hat{u}, \hat{v}), \tag{9}$$

where $\tilde{H}_{jk}(\hat{u}, \hat{v})$ is an adjoint Hermite polynomial in two variables (see Frenkiel & Klebanoff 1973).

The probability distribution of one variable is much simpler and is derived in the same manner as (7):

$$p(\hat{u}) = G(\hat{v}) + \sum_{j=3}^{4} (-1)^j \frac{Q_{j0}}{j!} \frac{\partial^j}{\partial \hat{u}^j} G(\hat{u}), \quad G(\hat{u}) \equiv \frac{1}{(2\pi)^{\frac{1}{2}}} \exp\left(-\frac{\hat{u}^2}{2}\right), \tag{10}$$

or

$$p(\hat{u}) = G(\hat{u})\{1 + \tfrac{1}{6}Q_{30}(\hat{u}^3 - 3\hat{u}) + \tfrac{1}{24}Q_{40}(\hat{u}^4 - 6\hat{u}^2 + 3)\}. \tag{11}$$

When all cumulants Q_{jk} in (7), (9) or (11) with $j+k \geqslant 3$ are equal to zero, the Gram–Charlier distribution becomes the same as the Gaussian one, and thus it may be said that Q_{jk} gives a measure of the skewness or intermittency of the distribution.

Now consider the probability distribution $p_w(w)$ of the normalized Reynolds stress $w \equiv uv/\overline{uv}$. By a change of variables (7*a*) may be reduced to

$$p_w(w) = \int_{-\infty}^{\infty} \frac{R}{|\hat{u}|}\, p(\hat{u}, -Rw/\hat{u})\, d\hat{u}$$

$$= \frac{R}{\pi(1-R^2)^{\frac{1}{2}}} \exp\left(\frac{R^2 w}{1-R^2}\right) \int_0^{\infty} \exp\left(-\frac{\hat{u}^2 + R^2(w/\hat{u})^2}{2(1-R^2)}\right)$$

$$\times \left[1 + \sum_{j+k=3}^{4} \frac{Q_{jk}}{j!\,k!} \tfrac{1}{2}\{H_{jk}(\hat{u}, -Rw/\hat{u}) + H_{jk}(-\hat{u}, Rw/\hat{u})\}\right] \frac{d\hat{u}}{\hat{u}}. \tag{12}$$

Since H_{jk} is an odd function for when $j+k$ is odd and vice versa, the third-order cumulants in the correction term of $p_w(w)$, i.e. the second term in (12), vanish. The third-order cumulants, which are closely connected with turbulent diffusion,

as will be mentioned later, are much more important quantities than the fourth-order cumulants. Furthermore, it has been pointed out by Lu & Willmarth (1973) that the $p_w(w)$ obtained by neglecting the cumulants of higher than third order, which is given by a Gaussian distribution in this case, agrees fairly well with experimental values. This may be due to the cancellation of terms including the third-order cumulant. Because they disregarded this third-order cumulant, some previous studies such as those by Lu & Willmarth (1973) and Antonia & Atkinson (1973) could find little obvious relation between the bursting process and the probability distribution of the Reynolds stress.

From the above description, a conditional probability distribution should be introduced in order to evaluate the effect of the third-order cumulants, while, for simplicity, the fourth-order cumulants, which are less important, may be omitted.

We shall denote the probability distributions of each event shown in figure 1 by $p_1(w)$ (outward interaction), $p_2(w)$ (ejection), $p_3(w)$ (inward interaction) and $p_4(w)$ (sweep), respectively. Therefore

$$p_w(w) = p_1(w) + p_2(w) + p_3(w) + p_4(w). \tag{13}$$

From (7) and (12), $p_i(w)$ ($i = 1, \ldots, 4$) can be derived by using conditional calculation. For example, $p_2(w)$ becomes

$$p_2(w) = \frac{R\exp(Rt)}{2\pi(1-R^2)^{\frac{1}{2}}}\int_0^\infty \exp\left\{-\frac{x^2+(t/x)^2}{2}\right\} \times\left[1-\frac{1}{(1-R^2)^{\frac{3}{2}}}\{A_1x^3-A_1^*(t/x)^3-A_2x^2(t/x)+A_2^*x(t/x)^2-A_3x+A_3^*(t/x)\}\right]\frac{dx}{x}, \tag{14}$$

where $t \equiv Rw/(1-R^2)$,

$$\left.\begin{aligned} A_1 &\equiv \tfrac{1}{6}Q_{30}+\tfrac{1}{2}RQ_{21}+\tfrac{1}{2}R^2Q_{12}+\tfrac{1}{6}R^3Q_{03},\\ A_2 &\equiv \tfrac{1}{2}RQ_{30}+(R^2+\tfrac{1}{2})Q_{21}+(R+\tfrac{1}{2}R^3)Q_{12}+\tfrac{1}{2}R^2Q_{03},\\ A_3 &\equiv \tfrac{1}{2}Q_{30}+\tfrac{3}{2}RQ_{21}+(R^2+\tfrac{1}{2})Q_{12}+\tfrac{1}{2}RQ_{03} \end{aligned}\right\} \tag{15}$$

and A_i^* is A_i with Q_{jk} replaced by Q_{kj}.

Now we have the following mathematical formulae:

$$\int_0^\infty \exp\left\{-\frac{x^2+(t/x)^2}{2}\right\}x^n(t/x)^m\frac{dx}{x} = t^m|t|^{\frac{1}{2}(n-m)}K_{\frac{1}{2}(n-m)}(|t|), \tag{16}$$

$$K_{\nu+1}(t) = 2\nu t^{-1}K_\nu(t)+K_{\nu-1}(t), \quad K_{-\nu}(t) = K_\nu(t), \tag{17}$$

where K_ν is the νth-order modified Bessel function of the second kind. Hence substitution of (15)–(17) into (14) yields

$$p_2(w) = p_G(w)+\psi^-(w) \quad (w > 0). \tag{18}$$

In the same manner,

$$p_1(w) = p_G(w)+\psi^+(w), \quad p_3(w) = p_G(w)-\psi^+(w) \quad (w < 0), \tag{19), (20}$$

$$p_4(w) = p_G(w)-\psi^-(w) \quad (w > 0), \tag{21}$$

where
$$p_G(w) = \frac{R}{2\pi} e^{Rt} \frac{K_0(|t|)}{(1-R^2)^{\frac{1}{2}}}, \tag{22}$$

$$\psi^+(w) = \frac{R}{2\pi} e^{Rt} K_{\frac{1}{2}}(|t|) \frac{|t|^{\frac{1}{2}}}{(1-R)^2} \left\{(1+R)\left(\frac{S^+}{3}+D^+\right)|t| - \left(\frac{2-R}{3}S^+ + D^+\right)\right\}, \tag{23}$$

$$\psi^-(w) = \frac{R}{2\pi} e^{Rt} K_{\frac{1}{2}}(t) \frac{t^{\frac{1}{2}}}{(1+R)^2} \left\{(1-R)\left(\frac{S^-}{3}+D^-\right)t - \left(\frac{2+R}{3}S^- + D^-\right)\right\} \tag{24}$$

and
$$S^{\pm} \equiv \tfrac{1}{2}(S_v \pm S_u) = \tfrac{1}{2}(Q_{03} \pm Q_{30}), \quad D^{\pm} \equiv \tfrac{1}{2}(D_v \pm D_u) = \tfrac{1}{2}(Q_{21} \pm Q_{12}). \tag{25}$$

S_u and S_v are the skewness factors of u and v respectively, as $S_u = \overline{\hat{u}^3}$ and $S_v = \overline{\hat{v}^3}$. D_u and D_v correspond to turbulent diffusion in the x and y directions respectively, as $D_u = \overline{\hat{u}.\hat{v}^2}$ and $D_v = \overline{\hat{v}.\hat{u}^2}$, and here we shall call them the diffusion factors.

Using the conditional probability $p_i(w)$ $(i = 1, \ldots, 4)$ and (13), $p_w(w)$ becomes $2p_G(w)$, in which $\psi^{\pm}$ disappear; then $p_w(w)$ coincides with a distribution directly derived from the Gaussian. Thus it is suggested that $\psi^{\pm}$ are very important terms for the sequence of the bursting process and that they are closely connected with the turbulent diffusion. When the pair (u, v) is transformed into $(-u, v)$, the aforementioned quantities change as follows: $R \to -R$, $S^- \to S^+$, $D^- \to D^+$, $w \to -w (t \to -t)$ and, consequently, $p_G(w) \to p_G(w)$ and $\psi^-(w) \to \psi^+(w)$. Hence, for example, $p_2(w)$ is transformed into $p_1(w)$, and thus an ejection event is transformed into an outward interaction event as expected in reality.

Next, taking into account the partition level H in the diagram of Reynolds stress $w = uv/\overline{uv}$ according to Lu & Willmarth (1973), as shown in figure 1 (*b*), the contributions to the Reynolds stress can be associated with one of five events including a hole event when $|w| < H$. The hole event is labelled event 5. Then the time fraction $T_i(H)$ and the contribution to the Reynolds stress $RS_i(H)$ corresponding to each event can be represented by

$$T_i(H) = \left\{ \begin{array}{l} \displaystyle\int_H^{\infty} p_i(w)\,dw \quad (i = 2, 4), \\ \displaystyle\int_{-\infty}^{-H} p_i(w)\,dw \quad (i = 1, 3), \end{array} \right\} \tag{26}$$

$$T_5(H) = \int_{-H}^{H} p_w(w)\,dw = 1 - \sum_{i=1}^{4} T_i(H) \quad \text{(the hole event)} \tag{27}$$

and
$$RS_i(H) = \left\{ \begin{array}{l} \displaystyle\int_H^{\infty} w p_i(w)\,dw > 0 \quad (i = 2, 4), \\ \displaystyle\int_{-\infty}^{-H} w p_i(w)\,dw < 0 \quad (i = 1, 3), \end{array} \right\} \tag{28}$$

$$RS_5(H) = \int_{-H}^{H} w p_w(w)\,dw = 1 - \sum_{i=1}^{4} RS_i(H) \quad \text{(the hole event)}. \tag{29}$$

When $H = 0$, the above equations describe the contribution of each event given by figure 1 (*a*). When $H > 0$, it may be expected that the characteristics of each event such as skewness and intermittency can be made clear. Also, some relationships between the coherent vortex motion with turbulent production which was

Case	h (cm)	Aspect ratio B/h	U_{max} (cm/s)	U_m (cm/s)	U_* (cm/s)	U'_* (cm/s)	$\frac{\lvert U_* - U'_* \rvert}{U_*}$ (%)	$Re = U_m h/\nu$ ($\times 10^4$)	$Fr = U_m/(gh)^{\frac{1}{2}}$	Slope S ($\times 10^{-4}$)	$k_s^+ = k_s U_*/\nu$	T_w (°C)
A	7.77	6.43	16.83	14·80	0·810	0·780	3·8	1·09	0·170	0·80	$\doteqdot 0$	18·35
B	7·94	6·29	17·69	15·45	0·895	0·939	4·8	0·98	0·175	1·13	9·1	11·35
C	7·88	6·34	15·69	13·22	0·989	0·999	1·0	0·98	0·150	1·23	48·0	17·95
D	7·63	6·55	17·21	13·87	1·336	1·416	6·6	0·86	0·160	2·77	136·2	12·30

TABLE 1. Hydraulic parameters for experiments. Friction velocity, U_*: from log law, $U'_* = (ghS)^{\frac{1}{2}}$. T_w = water temperature. $Re_\theta \simeq \frac{1}{10}Re \simeq 10^3$ if $\frac{1}{7}$-power velocity law is valid.

observed by Corino & Brodkey (1969) or Kim *et al.* (1971) through flow visualization and the data obtained in this study through point measurements may be discussed by varying H as a parameter.

3. Experimental equipment and data analysis

The experiments on two-dimensional fully developed turbulent flow in an open channel were conducted in a tilting flume 15 m long, 50 cm wide and 30 cm deep. The channel slope could be changed by adjusting two jacks so that normal flow could be obtained. A few baffles and screens to prevent the occurrence of large-scale disturbances were set up at the entrance of the channel, and consequently a fully developed turbulent flow was obtained at the test section 9·5 m downstream of the entrance.

Four kinds of bed roughness were chosen for the test: one smooth lucite bed (case A) and three rough beds (cases B, C and D) made of spherical glass beads with uniform diameter k_s spread densely over the bed (k_s represents the equivalent sand roughness of Nikuradse). The hydraulic parameters for each run are shown in table 1. Since the Reynolds number $Re = U_m h/\nu$ (where U_m is the mean velocity and h is the flow depth) and the Froude number $Fr = U_m/(gh)^{\frac{1}{2}}$ were kept nearly constant for all runs, it was expected that only the effects of roughness would be observed.

The streamwise and normal components of the instantaneous velocity were measured by using a set of constant-temperature anemometers with a DISA type 55A89 dual-sensor hot-film probe. To diminish the effects of variation of water temperature and impurities in the water upon the characteristics of the hot film, a stable water temperature was maintained during the operating period by circulating the water throughout the day before the test began, while the suspended materials in the flow were filtered by gauzes. The hot-film anemometers were calibrated by using both a Pitot tube and a float before and after each run. The calibration curves were obtained by the method given by Bradshaw (1971, chap. 8), the correction for the effect of water temperature being done by using the calibration coefficients.

The output signals of the anemometers were recorded in analog form by using an FM tape recorder and then were reproduced for conversion to digital form. In order to obtain 5000 samples at any measuring point, 100 Hz, 18 bit analog-to-digital conversions were conducted by using an analog-to-digital converter, FACOM U-200. Some statistical analysis was carried out by means of conditional sampling with a large digital computer, FACOM 230–75, Data Processing Center, Kyoto University.

The local mean velocities and some turbulence characteristics were obtained easily, and the mean velocity profile indicated a logarithmic law, by which the friction velocity U_* was evaluated as shown in table 1. Then, it was confirmed that the flow was two-dimensional and fully developed. A more detailed description of these results is given in Nagakawa *et al.* (1975).

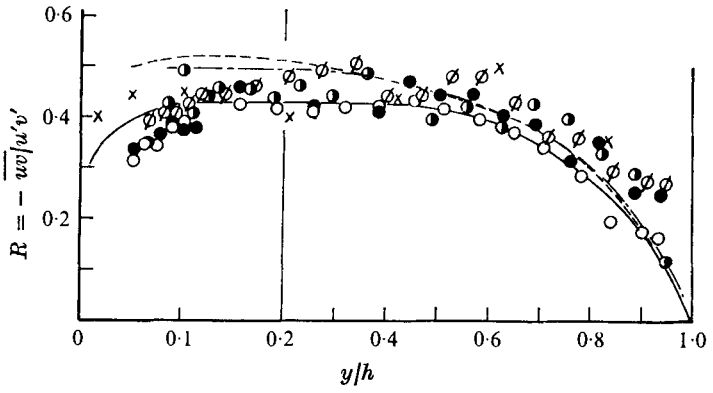

FIGURE 2. Correlation coefficients in turbulent open-channel flows. Present results: ○, $k_s^+ \doteqdot 0$ (smooth bed); ●, $k_s^+ = 9$ (incompletely rough bed); ∅, $k_s^+ = 48$ (incompletely rough bed); ◑, $k_s^+ = 136$ (completely rough bed). Laufer (1954): — – —, $Re = 1{\cdot}1 \times 10^4$ (smooth channel); – – – –, $Re = 2{\cdot}2 \times 10^4$ (smooth pipe). Bremhorst & Walker (1973): ——, $Re = (2{\cdot}3 - 9{\cdot}0) \times 10^4$ (smooth pipe). Lu & Willmarth (1973): ×, $Re = 4 \times 10^4$ (smooth boundary layer).

4. Experimental results and discussion

Correlation coefficients

The correlation coefficients $R = -\overline{uv}/u'v' > 0$ for the smooth bed (case A), the incompletely rough beds (cases B and C) and the completely rough bed (case D) are shown in figure 2 *vs.* y/h. In the wall region ($y^+ = U_* y/\nu < 100$ or $y/h \lesssim 0{\cdot}1$ in this case) and the free-surface region ($y/h > 0{\cdot}6$) respectively, R increases and decreases monotonically with y/h, while in the equilibrium region ($0{\cdot}1 < y/h < 0{\cdot}6$) it remains nearly constant.

The subdivision of turbulent flow field is discussed by Nagakawa *et al.* (1975). The comparison with previous data in pipe flow and boundary-layer flow shown in figure 2 indicates that R displays the universal characteristics, irrespective of the flow conditions and the roughness.

Probability density function and its higher moments

The data plotted in figure 3 are the probability densities measured in each region of turbulent flow over a smooth bed. Data were sampled by dividing the region $-3 < \hat{u}, \hat{v} < 3$ into 40 cells. When the skewness factor S and the flatness factor F are given, the Gram–Charlier distribution (11) is determined by using a relation such as $Q_{40} = F_u - 3$ from (5), and comparing this with the observed values. The experimental values of S and F for u and v are shown in figure 4, together with data obtained in a boundary layer by Gupta & Kaplan (1972) and in an oil flow by Kreplin (1973, quoted in Eckelmann 1974). Owing to the deficiency of measurements in the vicinity of the wall, it is difficult to make a definite remark about the difference in the values of these quantities in free-surface flow and in boundary-layer flow. But, except for the free-surface region, good agreement between the two may be observed. In this region both S and F have their

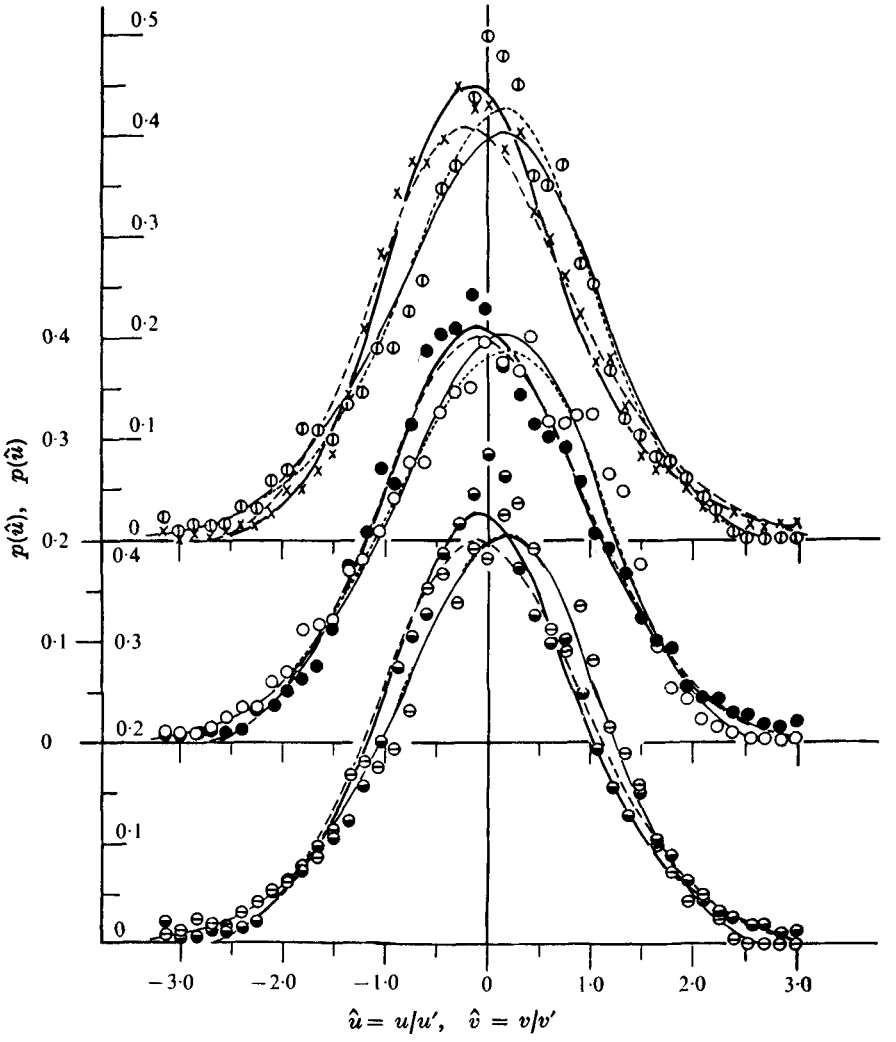

FIGURE 3. Probability density distributions of u and v (smooth bed). Measurements: ⊖, ◒, u, v at $y/h = 0{\cdot}064$; ○, ●, u, v at $y/h = 0{\cdot}193$; ⊙, ×, u, v at $y/h = 0{\cdot}772$. Theoretical curves [equation (11)]: ——, u (third order); – – –, v (third order); · · · · · · ·, u (fourth order); ——, v (fourth order).

maximum values, while they increase or decrease monotonically in the outer layer of the boundary-layer flow. This discrepancy may be due to the presence of large-scale intermittency in the boundary-layer flow.

It is noteworthy that S_u and S_v are almost symmetrical with respect to each other about the axis $S = 0$ (Gaussian) for any value of y^+, and change sign at $y^+ \simeq 10$. Also, figure 4 suggests that the Gram–Charlier distribution should be taken into account in both the wall and the free-surface regions because the deviation from the Gaussian distribution becomes larger in these regions.

The theoretical curves of the probability density given by (11) were calculated by using the measured values of S and F, and are shown in figure 3. Despite some

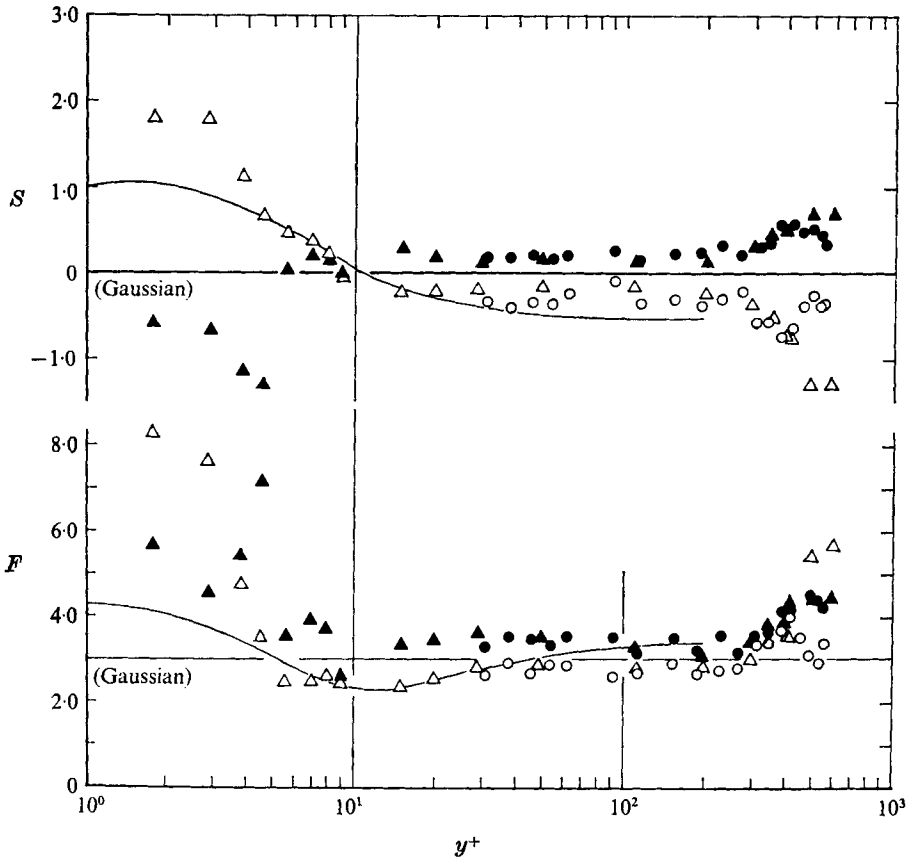

FIGURE 4. Distributions of skewness and flatness factors of u and v. Present results: ○, u; ●, v (open channel, $Re = 1{\cdot}1 \times 10^4$). Gupta & Kaplan (1972): △, u; ▲, v (boundary layer, $Re_\theta = 1900$; θ = momentum thickness). Kreplin (1973): ——, experimental curves of S_u and F_u (oil channel $Re = 4800$ and 7100).

scatter in the observed data, the actual phenomena can be fairly well explained by the Gram–Charlier distribution. Though the fourth-order distribution is in better agreement with the experimental results than the third-order one, the difference between the two does nothing to change the essential characteristics of the distribution. In the wall region, except for the viscous sublayer and the equilibrium region, the third-order distribution seems to be sufficiently accurate. But it is better to consider the fourth-order distribution for the free-surface region, where the deviation from the observed values becomes comparatively large. Like S_u and S_v, shown in figure 4, the distributions of $p(\hat{u})$ and $p(\hat{v})$ indicate nearly symmetrical deviation to the positive and negative sides of the zero axis respectively; $p(\hat{u})$ having its maximum value on the positive side and its longer tail on the negative side, and vice versa for $p(\hat{v})$.

The above description of the flow over the smooth bed applies in the case of the rough beds too. The values of the fourth- and fifth-order moments are shown in figure 5, as well as the data obtained by Lawn (1971). In the wall and equilibrium

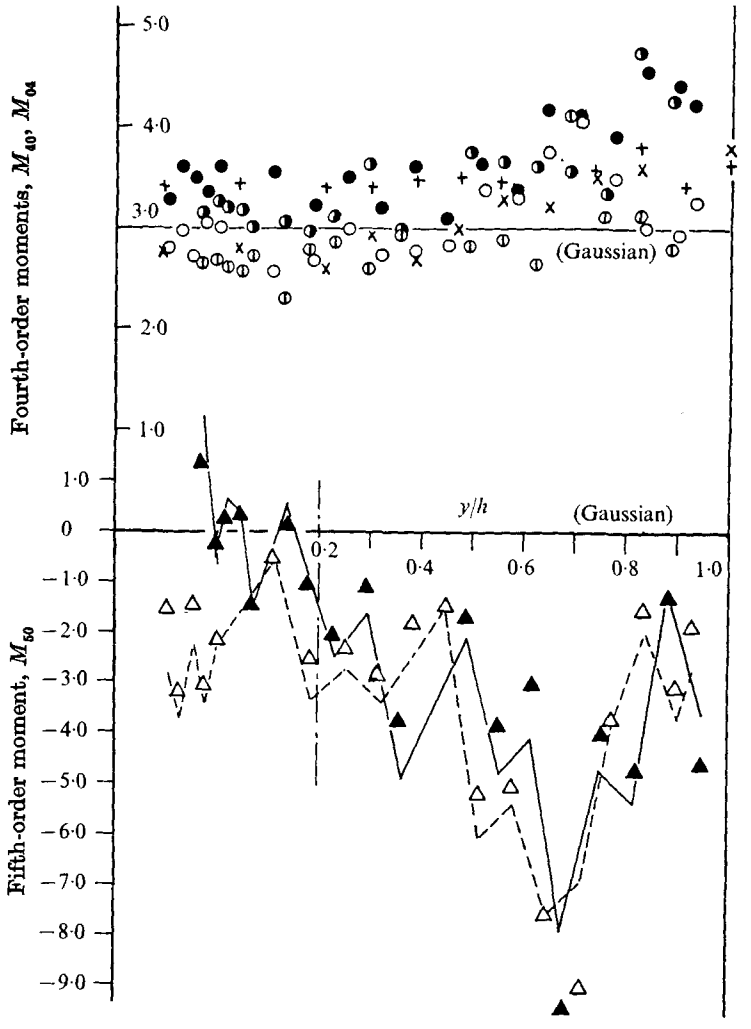

FIGURE 5. Distributions of the fourth- and fifth-order moments. Fourth-order moments of u and v: ○, ●, u, v (*smooth channel*, present results); ⓘ, ◑, u, v (rough channel, present results); ×, +, u, v (smooth pipe, Lawn 1971). Fifth-order moments of u: △, ▲, smooth, rough (observed); – – –, ——, smooth, rough [calculated from (30)].

regions the fourth-order moments hardly deviate from the Gaussian distribution and thus the third-order distribution may be valid in these regions. In the free-surface region, however, the third-order approximation may yield significant errors because of a considerable deviation from the Gaussian distribution.

Judging from figure 5, the fifth-order moments widely deviate from Gaussian distributions. The following can be deduced in the same way as (5):

$$Q_{50} = M_{50} - 10M_{30}. \tag{30}$$

The values of M_{50} calculated from (30) by setting Q_{50} equal to zero are shown in figure 5, and they agree fairly well with the observed values. This is the reason

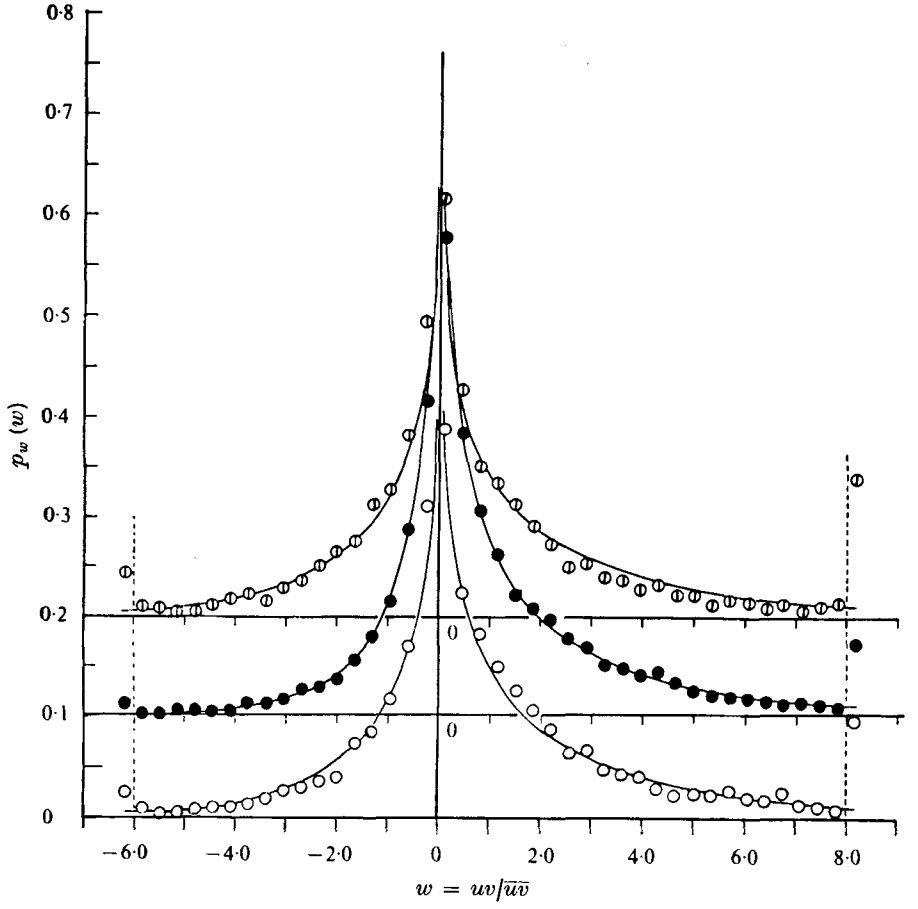

FIGURE 6. Probability density distributions of Reynolds stress (smooth bed). ○, y/h = 0·064, R = 0·351 (wall region); ●, y/h = 0·193, R = 0·420 (equilibrium region); ⊕, y/h = 0·772, R = 0·287 (free-surface region); ——, theoretical curves [equation (13)].

why the higher-order cumulants can be neglected as described in § 2. Since all the odd-order moments of a Gaussian distribution are equal to zero, it is suggested that the third-order Gram–Charlier distribution should replace the Gaussian one. Also, it seems that in the wall region the fifth-order moment is influenced by roughness, which will be discussed later in detail.

Probability density function of Reynolds stress

The observed values of the probability density function $p_w(w)$ of the Reynolds stress in each flow region are indicated in figure 6, as an example of the flow over a smooth bed. The fluctuating Reynolds stress $w\,(= uv/\overline{uv})$ was sampled by dividing $-6 < w < 8$ into 40 cells. The sums of the values of $p_w(w)$ in the ranges $w < -6$ and $w > 8$ respectively are plotted on the broken lines in figure 6. Since

$$p_w(w) = 2p_G(w)$$

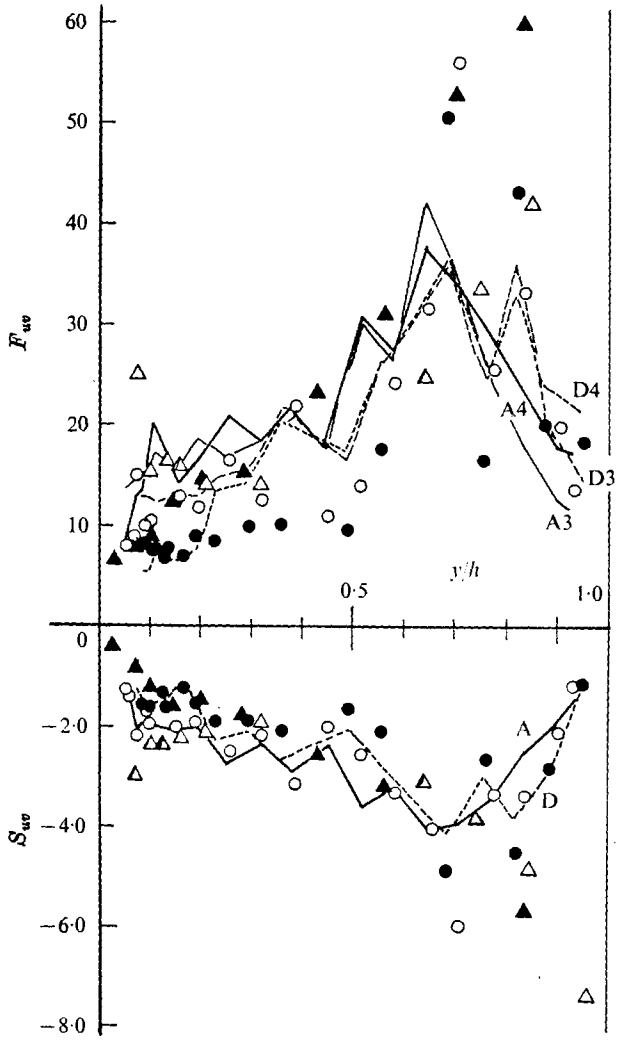

FIGURE 7. Distributions of skewness and flatness factors of uv. Observed: ○, smooth; ●, rough. Calculated from (31) and (32): ——, – – –, smooth, rough (third order); ——, - - - - - -, smooth, rough (fourth order). Antonia & Atkinson (1973), boundary layer: △, smooth; ▲, rough.

as indicated by (13), $p_w(w)$ was calculated by using the values of R given in figure 2, and the resulting curves are shown as solid lines in figure 6. Good agreement between the theoretical and experimental values was obtained, especially in the equilibrium region, and any small discrepancy between the two was due to a large deviation of the fourth-order moments from Gaussian as shown in figure 5. Consequently, the unconditional probability distribution $p_w(w)$ of Reynolds stress can be represented by one directly derived from a Gaussian distribution with high accuracy, as verified by Lu & Willmarth (1973) and Antonia & Atkinson (1973).

It may be noted from figure 6 that the probability distribution of values of uv has a very sharp peak at $w = 0$ and a very long tail extending to large values of $|w|$. In a theoretical equation $p_w(w)$ becomes infinite at $w = 0$ because $K_0(0) = \infty$ and becomes larger on the positive side of the curve than on the negative side because

$$\overline{w} = \int_{-\infty}^{\infty} w p_w(w)\, dw = 1.$$

Consequently, it can be suggested that almost all of the events occur with small values of $|w|$ but sometimes an event occurs with a very large value of $|w|$. Hence we can conclude that the instantaneous Reynolds stress might have marked intermittency.

In order to investigate this characteristic in detail, the observed values of the skewness factor S_{uv} and the flatness factor F_{uv} of w are shown in figure 7, together with data obtained by Antonia & Atkinson (1973). Provided that $Q_{jk} \equiv 0$ for $j+k \geqslant 5$, S_{uv} and F_{uv} can be evaluated in terms of the lower moments in the same way as in (5):

$$S_{uv} = \frac{1}{(M_{22}-R^2)^{\frac{3}{2}}}\{M_{30}M_{03} + 9M_{12}M_{21} + 3(M_{31}+M_{13}) + 2R(5R^2 - 3M_{22} + 9)\}, \quad (31)$$

$$\begin{aligned} F_{uv} = \frac{1}{(M_{22}-R^2)^2}\{&M_{40}M_{04} + 16M_{31}M_{13} + 24(M_{21}M_{03} + M_{12}M_{30}) \\ &+ 18(M_{22}^2 + 2M_{21}^2 + 2M_{12}^2) - 30R^2M_{22} \\ &+ 12R(M_{31} + M_{13} - 9M_{21}M_{12} - M_{30}M_{03}) - 3(R^4 + 24R^2 + 6)\}. \end{aligned} \quad (32)$$

The theoretical values of S_{uv} and F_{uv} were calculated from (31) and (32) by using the experimental values of the moments as indicated in figure 7. The calculated values are in comparatively good agreement with the observed ones. Some of the discrepancy in the F_{uv} diagram may be due to the error introduced by neglecting the higher-order cumulants.

As previously mentioned, the difference between the third-order distribution and the fourth-order one is not large. Both S_{uv} and F_{uv} show a gradual variation with y/h up to the equilibrium region, similar to the distribution of the higher-order moments shown in figure 5, but in the free-surface region they increase abruptly and then decrease towards the surface.

Although good agreement between the behaviour of S_{uv} and F_{uv} in open-channel flow and in boundary-layer flow can be seen up to the equilibrium region, in the free-surface region corresponding to the outer layer some discrepancies similar to those in figure 4 are evident. Since the absolute values of S_{uv} and F_{uv} are comparatively large in the free-surface region, the strong asymmetry and intermittency in the Reynolds-stress fluctuations may appear, as inferred from figure 6.

The effect of roughness on S_{uv} and F_{uv} seems to appear only in the wall region, so that their values for the rough beds become smaller than those for the smooth bed. This means that the profile of the $p_w(w)$ distribution is not so slender and the intermittency of the Reynolds-stress fluctuations is smaller in case of a rough bed.

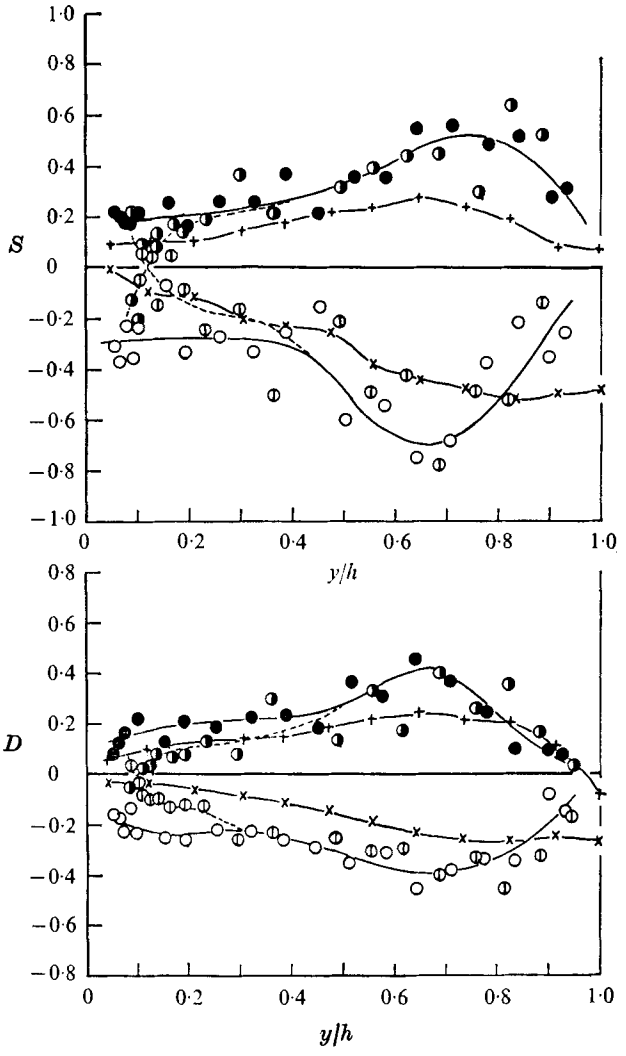

FIGURE 8. Distributions of skewness and diffusion factors of u and v. Present results: —○—, —●—, u, v (smooth, case A); - - - ◑ - - -, - - - ◑ - - -, u, v (rough, case D). Lawn (1971), smooth pipe: —×—, u; —+—, v.

Conditional probability distribution of Reynolds stress

As previously mentioned, $p_w(w)$ cannot describe the characteristics of each event separately, because some of the terms corresponding to different events may balance each other as indicated by (13). Thus the conditional probability density functions $p_i(w)$ ($i = 1, \ldots, 4$) expressed by (18)–(21) should be considered in order to discuss the contribution of each event to the Reynolds stress. This can be done by determining both the skewness factor S and the diffusion factor D connected with u and v, and their observed values for smooth and rough beds are shown in figure 8, together with data for a pipe flow obtained by Lawn (1971). Although the diffusion factor is smaller than the corresponding skewness factor, both

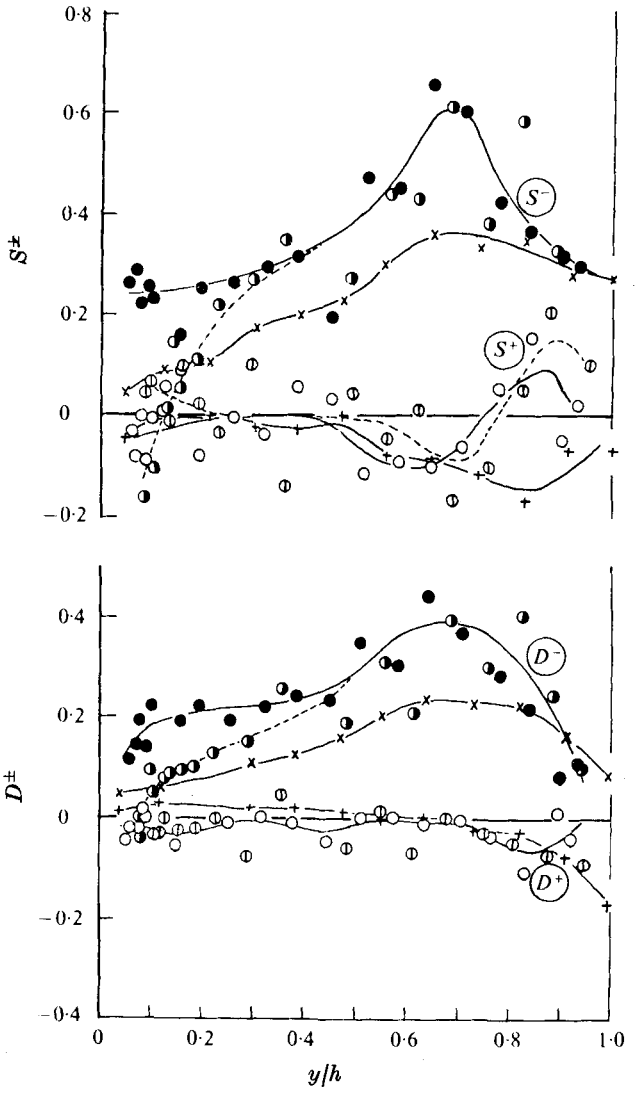

FIGURE 9. Distributions of S^+, S^-, D^+ and D^-. Present results: —○—, S^+, D^+ (smooth); —●—, S^-, D^- (smooth); – – –ⓘ– – –, S^+, D^+ (rough); – – –◑– – –, S^-, D^- (rough). Lawn (1971), smooth pipe: —+—, S^+, D^+; —×—, S^-, D^-.

curves are qualitatively similar and have the following characteristics. First, the relation between D_u and D_v resembles that between S_u and S_v, for example the D_u curve is almost the reflexion of the D_v curve in the zero axis. Also, $S_u < 0$, $S_v > 0$ and $D_u < 0$, $D_v > 0$ except in the immediate vicinity of the wall. Another characteristic seen in figure 8 is the remarkable effect of roughness in the vicinity of the wall. In case of the smooth bed, S and D both vary so gradually that they remain nearly constant when y/h is below the equilibrium region. For a rough bed the absolute values of S and D decrease towards the wall so rapidly that they become zero at $y/h \sim 0{\cdot}1$ and then, changing sign, increase upon approaching the

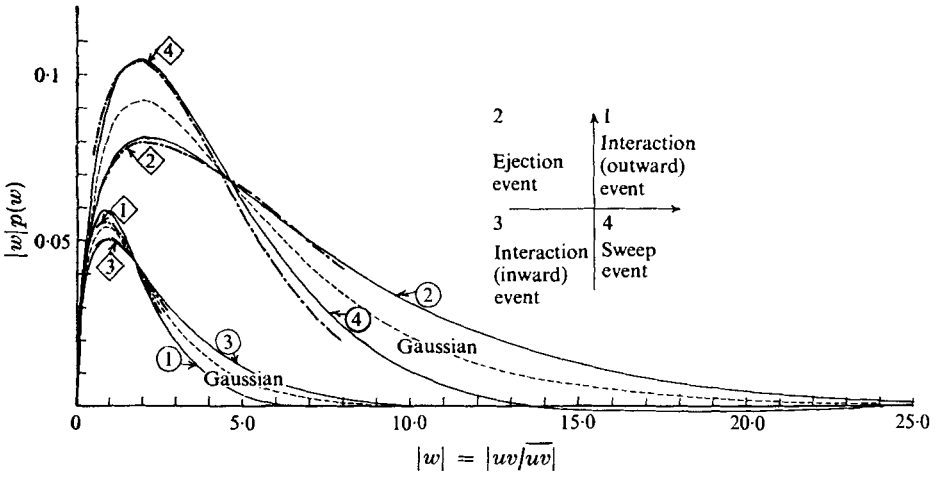

FIGURE 10. An example of the calculated conditional probability distributions of Reynolds stress (smooth bed). ——, calculated from (18)–(24) at $y/h = 0{\cdot}193$; —·—·—, observed by Brodkey *et al.* (1974) at $y/h = 0{\cdot}230$ ($y^+ = 45$).

wall. These trends are shown by the dashed lines in figure 8. Since in the middle of the equilibrium region the values of S and D for a rough bed always coincide with those for a smooth bed, it can be concluded that roughness has an effect on the values of S and D in this region at least.

In the free-surface region S and D both have a maximum value and decrease towards the free surface like the odd-order moments shown in figures 5 and 7. There is a close resemblance between our curves and Lawn's for a smooth bed except in the free-surface region. The difference in magnitude over the whole depth between our curves and Lawn's may be caused by the difference in data processing. As mentioned by Frenkiel & Klebanoff (1967), the analog method used by Lawn cannot be expected to obtain such accurate values of the higher-order moments as the digital procedure adopted here.

S^+, D^+, S^- and D^- can be evaluated from (25) for the values of S and D obtained above and are shown in figure 9. Judging from (25), and the symmetry between S_u and S_v and D_u and D_v in figure 8, S^+ and D^+ will reduce to nearly zero, and S^- and D^- to S_v and D_v respectively. The roughness effect is marked for S^- and D^- over the equilibrium region, while neither S^+ nor D^+ displays this effect because of cancellation of the roughness terms. By substituting the values of S^+, D^+, S^- and D^- into (18)–(24) with the Bessel function $K_{\frac{1}{2}}(t)$ equal to $(\pi/2t)^{\frac{1}{2}}\,e^{-t}$, the conditional probability distributions of the Reynolds stress can be obtained. An example of the calculated distribution for each event is presented in figure 10. The probability distribution at the point $y/h = 0{\cdot}193$ in the equilibrium region over a smooth bed is represented in terms of $|w|p(w)$. Similar figures have been obtained in the other regions and for rough beds. These theoretical results agree very well with the observations by Brodkey *et al.* (1974, figure 9).

In figure 10 both the ejection and the sweep events exhibit much larger values and much longer tails than the interaction events, which implies that the ejection and sweep events have much greater intermittency. Despite having a smaller

maximum, the curve of the ejection events has larger values than that of the sweep events beyond $w \simeq 5$, so that it may be expected that ejections make the greatest contribution to the Reynolds stress. Since $|w|\,p_1(w)$ is similar to $|w|\,p_4(w)$ while $|w|\,p_2(w)$ is similar to $|w|\,p_3(w)$, the characteristics of these events mainly depend upon the sign of u. This gives theoretical support to the observation by Brodkey *et al.* (1974) that the bursting process may be governed by the fluctuating velocity u rather than by v.

The fact that $wp_4(w)$ in figure 10 takes small negative values for large values of w is unreasonable, and therefore the sweep events cannot be represented accurately by (21) in this range of w. This negative $p_4(w)$ would probably be corrected by considering terms of higher than third order which have been described earlier. Thus the discrepancy between the experimental results and the theoretical values predicted by the third-order approximation will become larger near the free surface, where S_{uv} and F_{uv} are large.

The fraction of time $T_i(H)$ and the contribution to the Reynolds stress $RS_i(H)$ corresponding to each event in the flow over a smooth bed are shown in figures 11(*a*), (*b*) and (*c*) for a typical point in the wall, equilibrium and free-surface regions respectively.

Theoretical curves were obtained from (26)–(29), while our experimental data were analysed by almost the same method of conditional sampling as that used by Lu & Willmarth (1973):

$$T_i(H) = \lim_{T\to\infty} \frac{1}{T} \int_0^T I_i(t, H)\, dt \quad (i = 1, 2, 3, 4), \tag{33}$$

$$RS_i(H) = \frac{1}{\overline{uv}} \lim_{T\to\infty} \frac{1}{T} \int_0^T u(t).v(t)\, I_i(t, H)\, dt, \tag{34}$$

where

$$I_i(t, H) = \begin{cases} 1 & \text{for } |w(t)| > H \text{ and the point } (u, v) \text{ in the } i\text{th quadrant,} \\ 0 & \text{for } |w(t)| \leqslant H. \end{cases} \tag{35}$$

In the wall region (figure 11*a*) and the equilibrium region (figure 11*b*), the agreement between the experimental data and the predicted values is fairly good over a wide range of hole size H, so that it may be expected that the third-order probability distribution represents the correct picture for a sequence of bursting processes. In the free-surface region (figure 11*c*), however, a discrepancy between the two appears for large values of H, owing to the neglect of higher-order terms.

Although the time occupied for $H < 1$ amounts to about a half of the total time, the corresponding contribution to the Reynolds stress is only a few per cent, which suggests that $w(t)$ has a large intermittency. Though the inward interaction shows slightly larger values than the outward interaction, they both become negligibly small at $H \simeq 7$, and consequently the negative contribution to the Reynolds stress disappears. The sweep event decreases rapidly with H and beyond $H \simeq 10$ only the ejection event contributes to the Reynolds stress, while the time occupied by this event is very short. From this it may be inferred that the ejection event may arise in the form of a very sharp pulse, which agrees well with the results obtained by Corino & Brodkey (1969), Kim *et al.* (1971) or Grass (1971) by means of flow visualization.

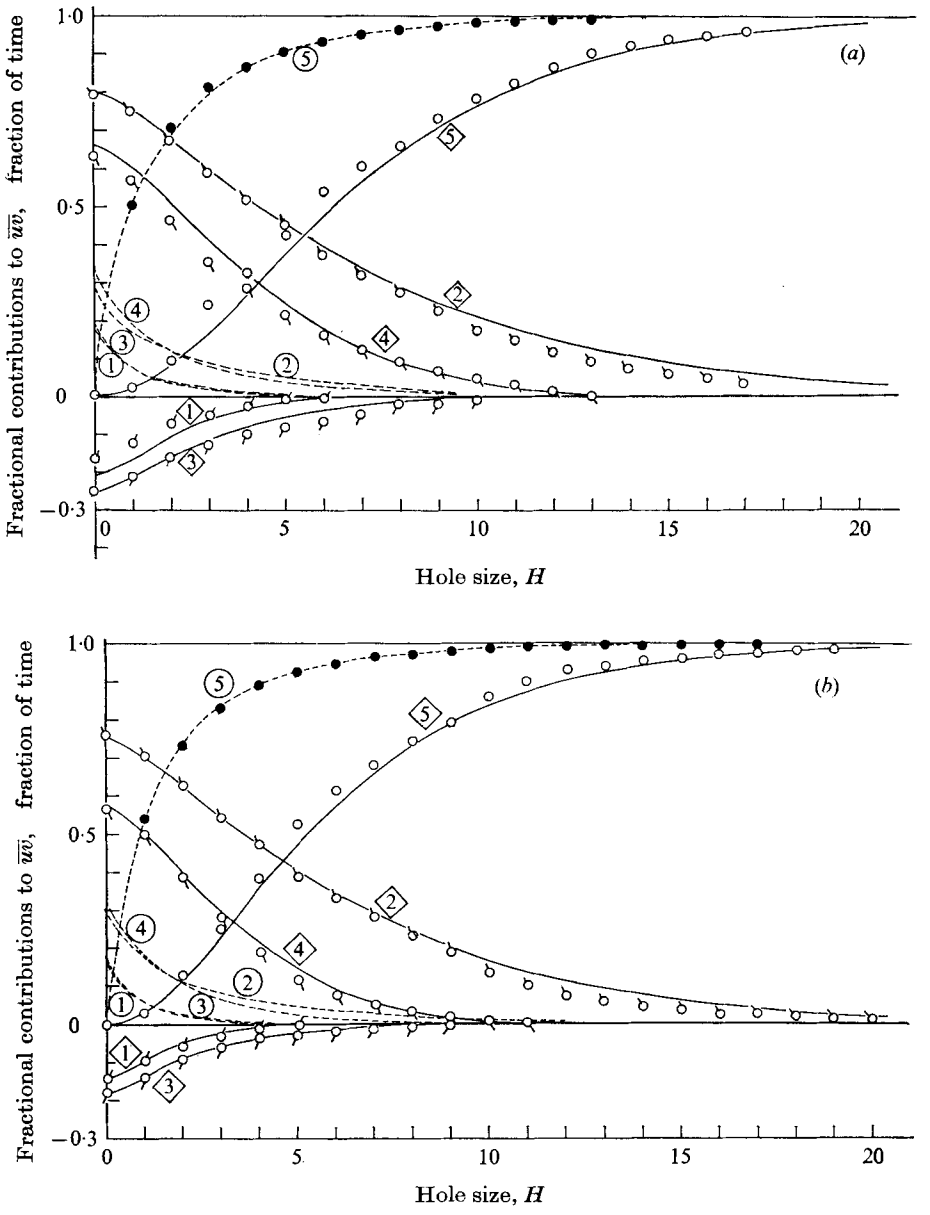

FIGURES 11 (*a*, *b*). For legend see facing page.

The correlations in magnitude among the four events are invariant over the whole depth. $RS_i(H)$ shows much larger values in the free-surface region than in other regions, while the $T_i(H)$ in each region nearly coincide with each other, so that $T_2 \simeq T_4$ and $T_1 \simeq T_3$. In particular, the fact that $T_2 < T_4$ and $RS_2 > RS_4$ for small values of H implies that the ejection event is more intensive than the sweep event in this range.

A typical example of the conditional probability distribution of the Reynolds

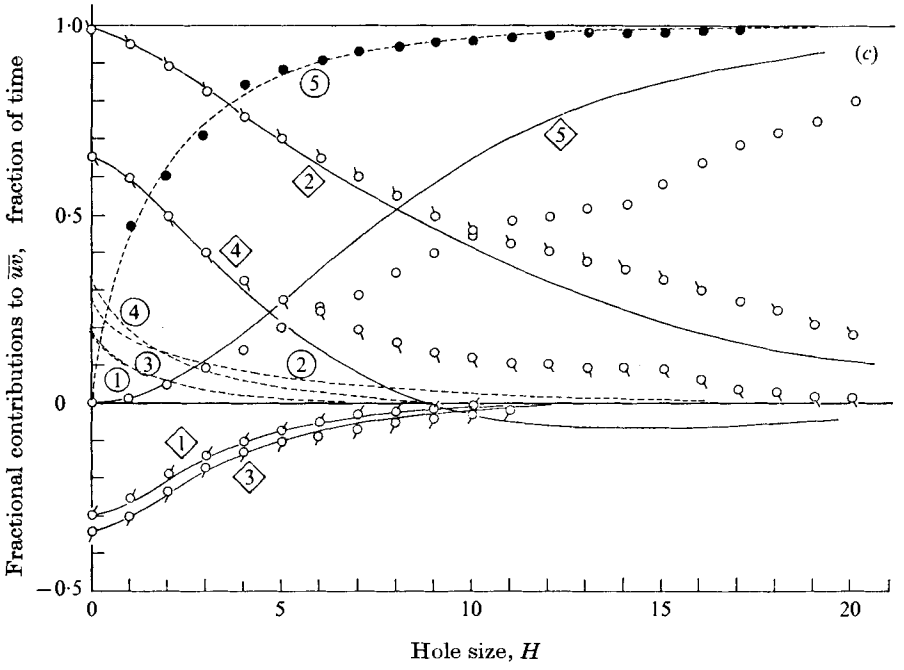

FIGURE 11. Fractional contributions to Reynolds stress and fraction of time occupied by each event (smooth bed). ⓘ, fraction of time occupied by ith event; ◈, fractional contribution to $-\overline{uv}$ from ith event. Observed values: ♂, RS_1; ♁, RS_2; ♀, RS_3; ♀, RS_4; ○, RS_5; ●, T_5. ——, – – – –; calculated curves from (26)–(29). (*a*) Wall region ($y^+ = 38$); $S^+ = -0{\cdot}090$, $D^+ = -0{\cdot}026$, $S^- = 0{\cdot}292$, $D^- = 0{\cdot}151$ and $R = 0{\cdot}351$. (*b*) Equilibrium region ($y/h = 0{\cdot}193$); $S^+ = -0{\cdot}089$, $D^+ = -0{\cdot}026$, $S^- = 0{\cdot}254$, $D^- = 0{\cdot}231$ and $R = 0{\cdot}420$. (*c*) Free-surface region ($y/h = 0{\cdot}772$); $S^+ = 0{\cdot}064$, $D^+ = -0{\cdot}035$, $S^- = 0{\cdot}423$, $D^- = 0{\cdot}289$ and $R = 0{\cdot}287$.

stress in the flow over a rough bed is presented in figure 12, together with the experimental results. Since the roughness effect appears predominantly in the wall region as indicated by our previous research, only the structure of the Reynolds stress in this region is discussed here; it was verified that the structure in the other regions was almost the same as that for a smooth bed, shown in figure 11. The agreement between the theoretical curves and the experimental values is fairly good. It is noteworthy that the relations between the magnitudes of the ejection and the sweep and between the magnitudes of the inward and the outward interactions become the reverse of those for a smooth bed because of the negative values of S^- and D^-. This result will be discussed in detail later.

Relative intensity of the different events

In order to describe clearly the relation between the sequence of the bursting process and the Reynolds stress, it is necessary to investigate the relative intensity of each event at $H = 0$. Figures 13(*a*) and (*b*) show the distributions of the Reynolds stress contributed by each event *vs.* y/h for the smooth and rough beds respectively. Experimental results for a smooth boundary layer by Lu &

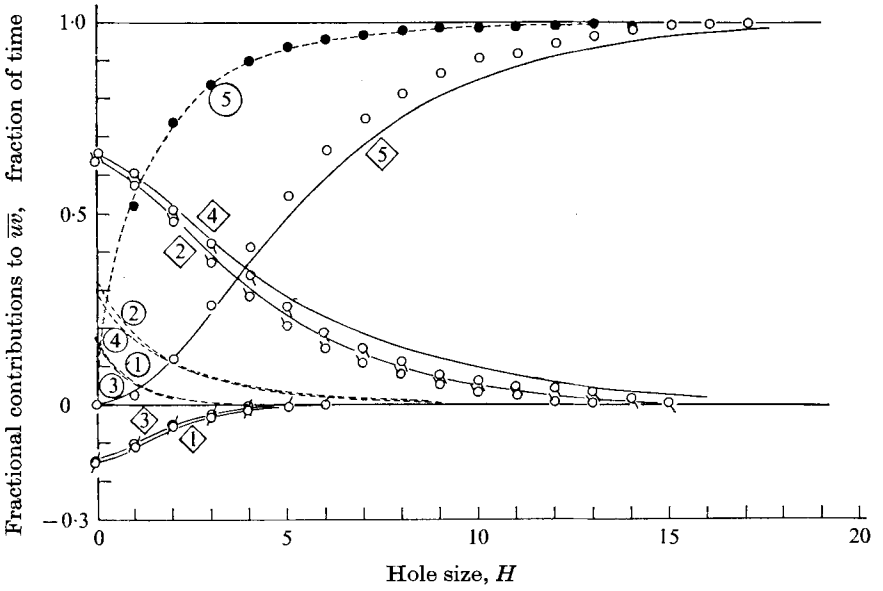

FIGURE 12. Fractional contributions to Reynolds stress and fraction of time occupied by each event (rough bed). Wall region ($y^+ = 71$ or $y/h = 0{\cdot}085$); $S^+ = 0{\cdot}050$, $D^+ = 0{\cdot}0$, $S^- = -0{\cdot}181$, $D^- = -0{\cdot}042$ and $R = 0{\cdot}431$. Notation as in figure 11.

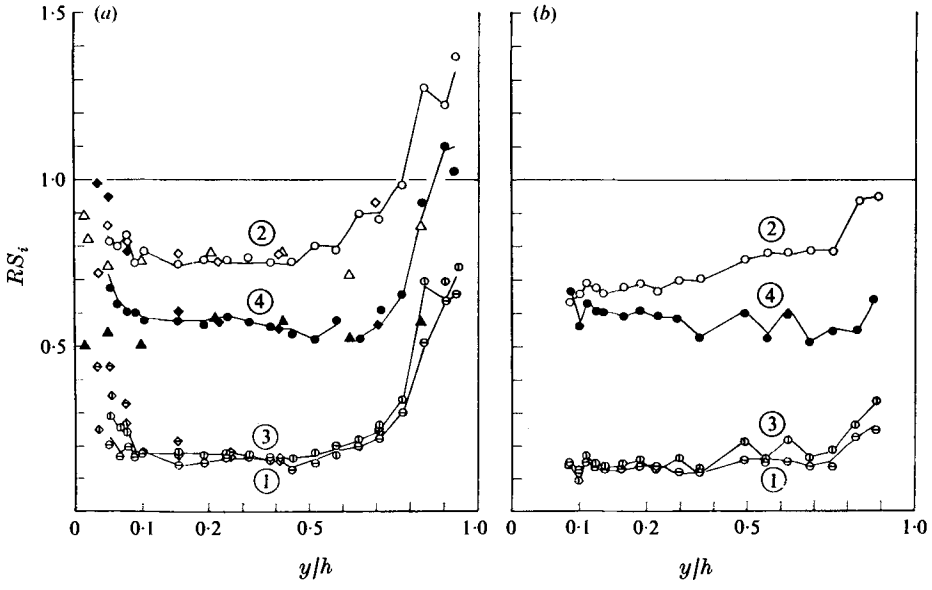

FIGURE 13. Distributions of contributions to Reynolds stress from different events with $H = 0$. (*a*) Smooth bed (case *A*). (*b*) Rough bed (case *D*). Present results: ⊖, $-RS_1$; ○, RS_2; ⓘ, $-RS_3$; ●, RS_4; ——, calculated from (28).Brodkey *et al.* (1974), oil channel: ◇, $-RS_1$; ◇, RS_2; ◇, $-RS_3$; ◆, RS_4. Lu & Willmarth (1973), boundary layer: △, RS_2; ▲, RS_4.

Willmarth (1973) and for a smooth oil channel by Brodkey *et al.* (1974) are also shown. It is very interesting that the observed values completely agree with the curves calculated from (28) over the whole depth, irrespective of the roughness size. This implies that the theoretical considerations in § 2 may be able to explain the bursting phenomenon in some detail for both rough and smooth beds.

In case of the smooth bed, there exists the relation ejection > sweep > inward interaction > outward interaction within the observed range of y/h. The difference between the two interactions, however, is almost negligibly small because $S^+ \simeq D^+ \simeq 0$ on the basis of the symmetry between S_u and S_v and between D_u and D_v in (25). In the wall region the intensities of all events decrease with increasing y/h, and good agreement was obtained between our results and those by Brodkey *et al.* (1974). Although the values of the ejection given by Lu & Willmarth (1973) agree well with our data, the values of the sweep show some differences. This discrepancy will be discussed later, with the characteristic quantities in the wall region represented by a y^+ parameter.

Next, in the equilibrium region, the intensity of each event is nearly constant irrespective of y/h. Since in this region a dynamic equilibrium exists between the turbulence production and dissipation, and a similarity in turbulent structure is expected to exist independently of external boundary conditions, it is expected that the bursting process and the accompanying turbulence production may attain a stable equilibrium state in this region, resulting in almost constant intensity for each event. The rates of intensity contributed by ejections and sweeps are about 75 % and 60 % respectively, and the excess Reynolds stress balances the sum of the negative rates contributed by the inward and outward interactions. Similar characteristics were verified by point measurements by Lu & Willmarth (1973) or Brodkey *et al.* (1974) and by flow visualization by Corino & Brodkey (1969) or Kim *et al.* (1971).

In the free-surface region the intensity of each event rapidly increases with y/h. Near the free surface both ejections and sweeps show a positive stress of over 100 %, while the negative stress brought about by the interactions increases to such an extent that the differences between the positive stress and the negative stress are equal to the net Reynolds stress.

The relations between the intensities of each event in case of the rough beds and the smooth bed are almost the same, as shown in figure 13 (*b*), so that we can confirm the observation by Grass (1971) that both ejections and sweeps exist irrespective of the roughness conditions. But, in the range from the wall to the middle of the equilibrium region, where the roughness effect on the turbulence structure may be expected to appear, some differences in the intensity profiles for the rough and smooth beds can be observed. It is noteworthy that, contrary to the case of a smooth bed, the intensity of ejections decreases towards the wall to become nearly equal to that of the sweeps at $y/h \simeq 0{\cdot}1$, and sweeps may become more intense than ejections in the vicinity of the wall as was observed by Grass (1971) using the hydrogen-bubble technique. This fact that both ejections and sweeps, which are the predominant events in the bursting phenomenon, may be greatly affected by the roughness condition is very important and will be discussed in detail later.

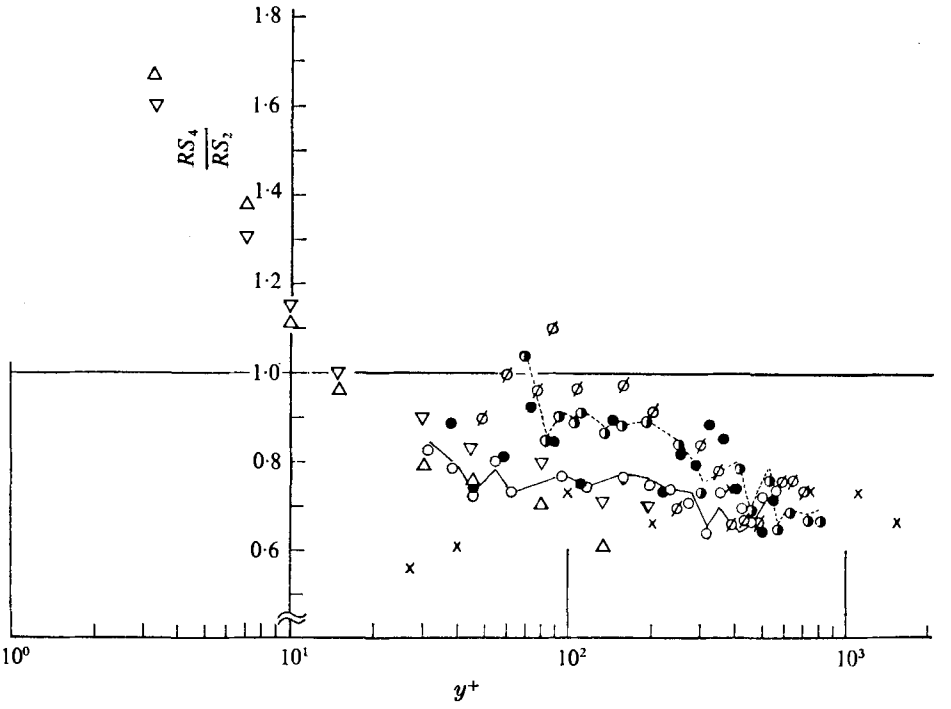

FIGURE 14. The ratio RS_4/RS_2 with $H = 0$ as a function of y^+. Present results, open channel, $Re \doteqdot 1{\cdot}1 \times 10^4$: ○, case A ($k_s^+ \doteqdot 0$); ●, case B ($k_s^+ = 9$); ∅, case C ($k_s^+ = 48$); ◑, case D ($k_s^+ = 136$). Present calculations: ——, case A; - - - - - -, case D. ▽, Wallace *et al.* (1972), oil channel, Re_θ low; △, Brodkey *et al.* (1974), oil channel, Re_θ low; ×, Lu & Willmarth (1973), boundary layer, $Re_\theta = 4200$.

The ratio RS_4/RS_2 of the Reynolds stress of a sweep to that of an ejection is plotted in figure 14, for each degree of roughness, with the results obtained by Wallace *et al.* (1972), Brodkey *et al.* (1974) and Lu & Willmarth (1973). In our experiments, for $y^+ > 100$ and case of a smooth bed RS_4/RS_2 remains nearly constant, the Reynolds stress of sweeps being about 70 % of that of the ejections, showing a good agreement with data by other investigators. For $y^+ < 100$, our values increase towards the wall like those of Wallace *et al.* (1972) or Brodkey *et al.* (1974), while the values by Lu & Willmarth (1973) show the reverse tendency, decreasing towards the wall. Lu & Willmarth suggested that this discrepancy might be due to the difference in the Reynolds number.

Assuming that S^+ and D^+ are both approximately zero on account of the symmetry of S and D and that D^-/S^- is nearly constant and equal to 0·7 (judging from figure 9), the curves of RS_4/RS_2 against S^- for different values of R can be calculated from (28); these results are shown in figure 15. A definite conclusion on the bursting process over the whole depth may not be drawn owing to the lack of data on the diffusion factor D in the vicinity of the wall. But if the above assumptions can be made here, it can be seen that RS_4/RS_2 may rather increase towards the wall because S^- is considered to decrease as it approaches the wall because of the variation of the skewness factor S shown in figure 4. Compared with figure 14,

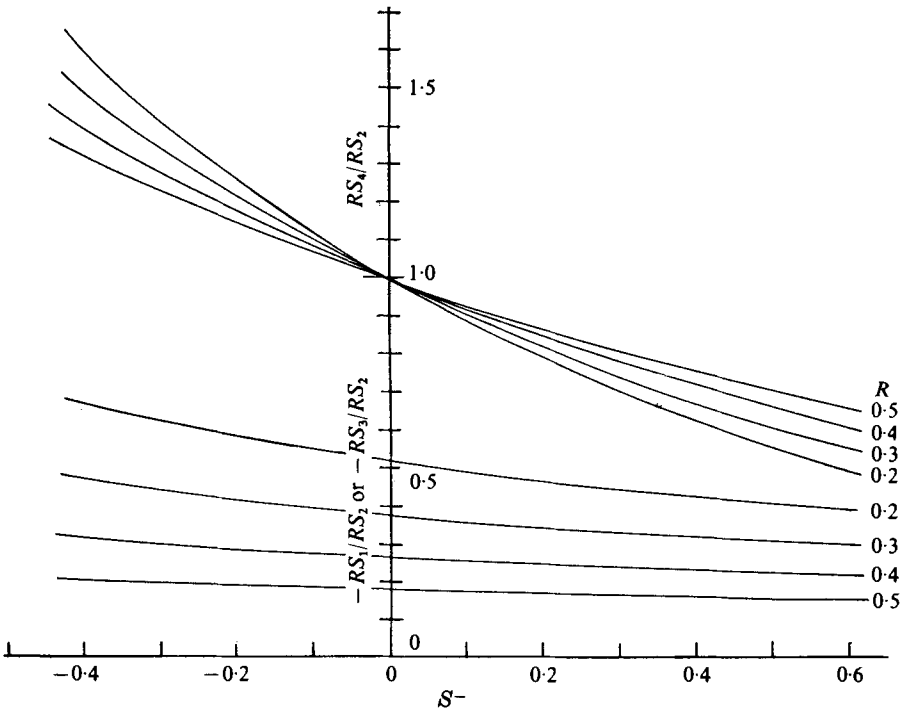

FIGURE 15. Calculated fractional contributions to Reynolds stress. $D^-/S^- = 0{\cdot}7$, $S^+ = D^+ = 0{\cdot}0$.

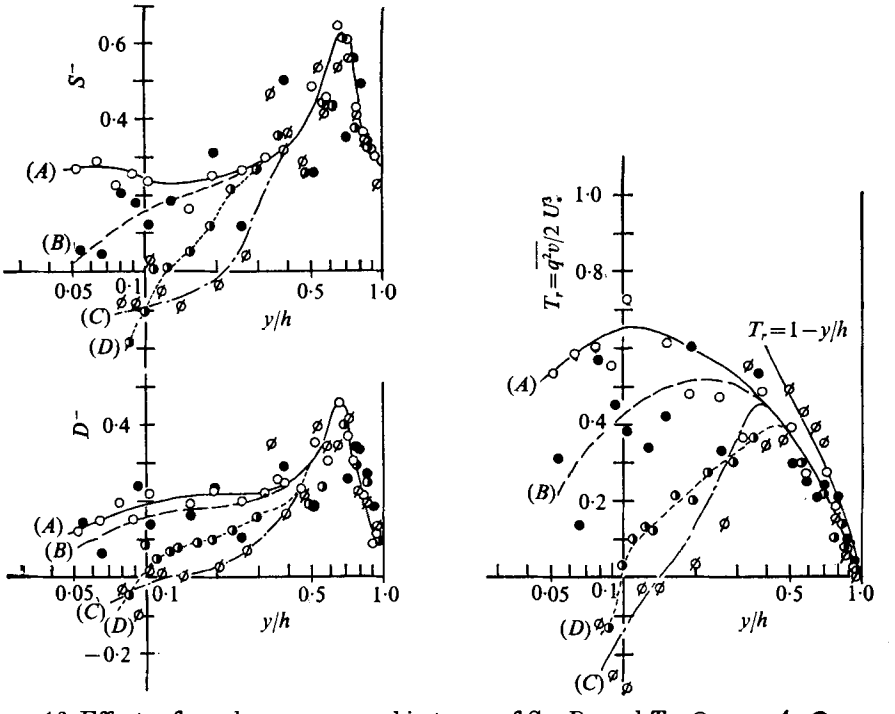

FIGURE 16. Effects of roughness expressed in terms of S^-, D^- and T_r. ○, case A; ●, case B; ⌀, case C; ◑, case D.

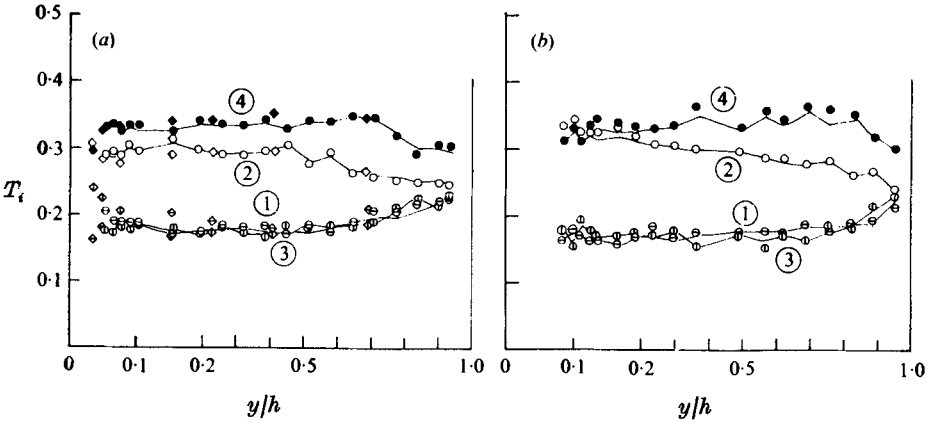

FIGURE 17. Distributions of fraction of time occupied by each event with $H = 0$. (*a*) Smooth bed (case *A*). (*b*) Rough bed (case *D*). Present results: ⊖, T_1; ○, T_2; ⓘ, T_3; ●, T_4; ——, calculated from (26). Brodkey *et al.* (1974), oil channel: ⟐, T_1; ◇, T_2; ◈, T_3; ◆, T_4.

the calculated curves represent well the experimental results in the wall region. The fact that the contribution of sweeps becomes larger than that of the ejections as the wall is approached is also suggested by the results obtained by Zarič (1972). Judging from the above, a tendency for the values of RS_4/RS_2 in the vicinity of the wall to decrease towards the wall, as indicated by Lu & Willmarth, seems to be incorrect.

Our data show that in the wall region the values of RS_4/RS_2 increase in proportion to the roughness scale, while in the outer part of the wall region the roughness effect diminishes with increasing y^+ and the same turbulence structure as in the flow over a smooth bed is seen in figure 14. This roughness effect on the Reynolds stress is due to the variation of the skewness factor S and the diffusion factor D with roughness. As shown in figure 15, S^- and D^- both decrease with increasing roughness in the range from the wall to the middle of the equilibrium region, which results in the increase of RS_4/RS_2 shown in figure 15. Thus the experimental results shown in figure 14 can be reasonably explained.

Defining $T_r = \overline{q^2 v}/2U_*^3$ as the turbulent energy transport, where $\frac{1}{2}\overline{q^2}$ is the turbulent kinetic energy, the following equation can be derived:

$$T_r \simeq \tfrac{1}{2}(v'/u')\,(u'/U_*)^3\{Q_{21} + 2(v'/u')^2 Q_{03}\}. \tag{36}$$

Since $Q_{21} \simeq D^-$, $Q_{03} \simeq S^-$ and $v'/u' \simeq 0{\cdot}55$ was obtained by the authors (1974), (36) is reduced to the following, independent of the roughness condition:

$$T_r \simeq 0{\cdot}28(u'/U_*)^3(D^- + 0{\cdot}6S^-). \tag{36a}$$

Figure 16 shows the values of T_r calculated from (36) using the measured velocity fluctuations. As mentioned in Nakagawa *et al.* (1975), the roughness effect is marked on this kind of figure. We can see from (36*a*) that T_r depends upon the values of D^- and S^- and so it decreases with increasing roughness. Since $\partial T_r/\partial y$ is directly involved in the turbulent energy budget as the term representing turbulent energy diffusion, it is expected that the bursting corresponding to the

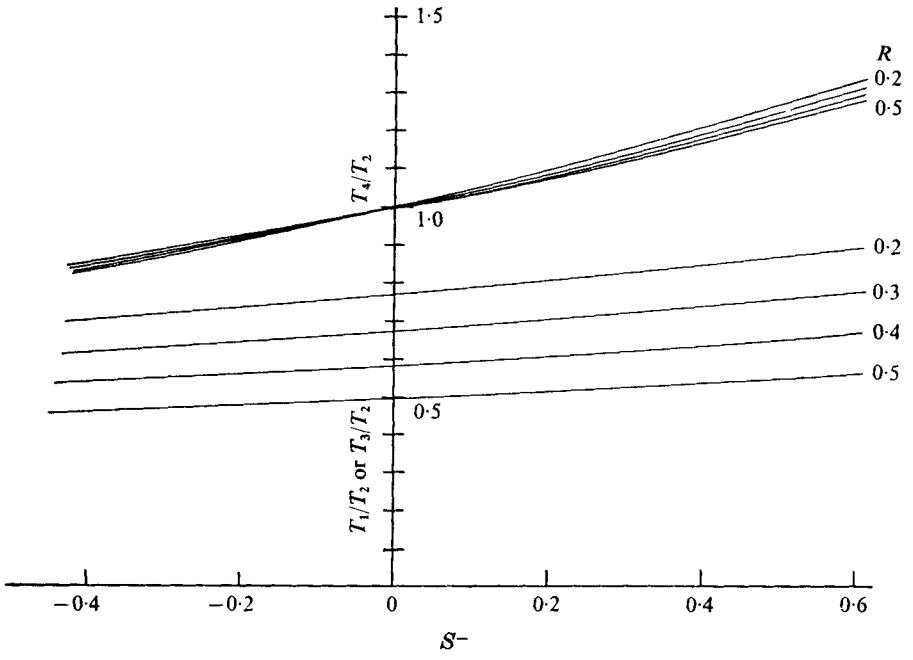

FIGURE 18. Calculated fraction of time. $D^-/S^- = 0{\cdot}7$, $S^+ = D^+ = 0{\cdot}0$.

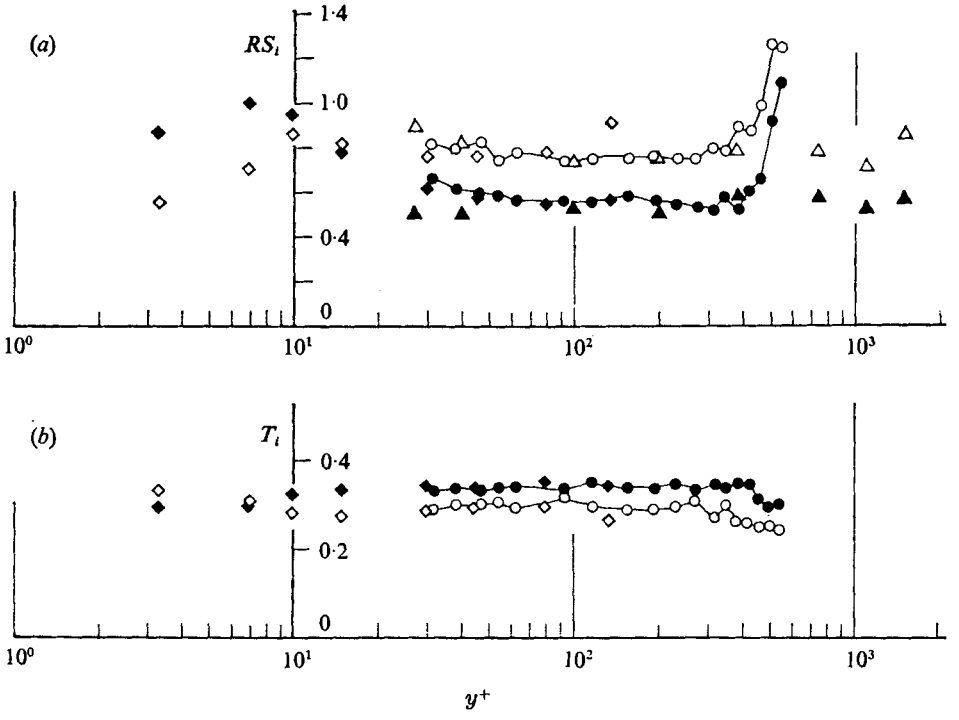

FIGURE 19. Distributions of (*a*) RS_i and (*b*) T_i for ejections and sweeps in the wall region ($y^+ < 100$). Present results: ○, ejection; ●, sweep; ——, calculated curves. Brodkey *et al.* (1974): ◇, ejection; ◆, sweep. Lu & Willmarth (1973): △, ejection; ▲, sweep.

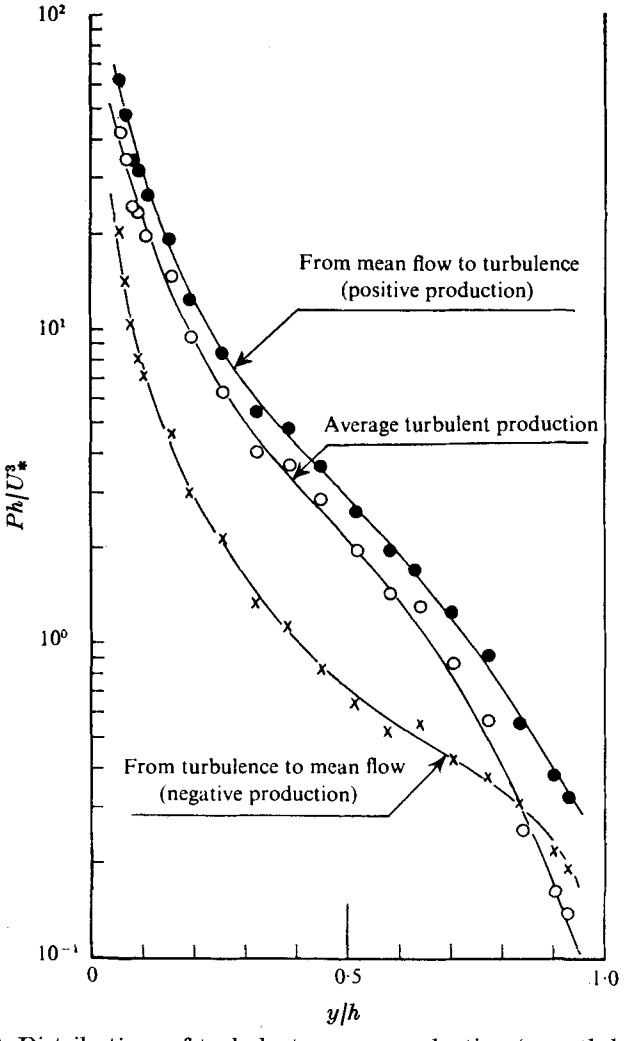

FIGURE 20. Distributions of turbulent energy production (smooth bed). ●, positive production; ×, negative production; ○, net production.

ejection or sweep motion is closely connected with the turbulent energy budget in the form of the turbulent diffusion.

The fractions of time occupied by each event on the smooth and rough beds are shown in figures 17(*a*) and (*b*), respectively, together with the theoretical curves calculated from (26). Unlike RS_i, the magnitude of the fraction of time T_i satisfies the relation sweep > ejection > outward interaction $\simeq$ inward interaction. Also, these results agree very well with those obtained by Brodkey *et al.* (1974). Each fraction of time is nearly constant irrespective of y/h except in the free-surface region, where the fractions of time for all events tend to approach a definite value on the free surface. It may be seen from this characteristic as well as that of RS_i that the bursting process near the free surface may consist of smoother and more isotropic events. The ratios of each fraction of time, which have been calculated in the same manner as in figure 15, are shown in figure 18.

T_4/T_2 increases with increasing S^- and is hardly affected by the variation of R, which can also describe the observed data reasonably.

The distributions of RS_i and T_i for the ejection and sweep in the wall region are shown in figures 19(*a*) and (*b*) respectively. Our data agree very well with the results obtained by Brodkey *et al.* Though some of the characteristics of these parameters have already been discussed, a remarkable aspect should be noticed: the relation in magnitude between the ejection and sweep may reverse at $y^+ \simeq 10$, which corresponds to the edge of the viscous sublayer. This characteristic can be predicted by the theory developed in § 2, using the distributions of the skewness factors of u and v shown in figure 4.

Lastly, the turbulent energy production $P = -\overline{uv}(\partial U/\partial y)$ is plotted *vs.* the flow depth in figure 20. The positive and negative time-average production are given by $(RS_2 + RS_4)P$ and $(RS_1 + RS_3)P$, respectively. The contribution of negative production to the net production is comparatively small up to the equilibrium region, but in the free-surface region it becomes of the same order as that of the net production though its absolute value is very small. It can be concluded, therefore, that the energy interchange from turbulence to the mean flow should not be neglected in the free-surface region. This property has been suggested by Hino, Sawamoto & Takasu (1975) even in an oscillating pipe flow.

5. Conclusions

In this paper the conditional probability distributions of the Reynolds stress have been deduced from a third-order joint distribution of u and v of Gram–Charlier type. In addition, how various events in the bursting process contribute to the Reynolds stress has been investigated. The turbulent fluctuations in an open-channel flow over smooth and rough beds have been measured by dual-sensor hot-film anemometers and the relations among these events in the bursting process have been investigated by conditional sampling of their signals. Thus we have confirmed that even the third-order probability distribution of the Reynolds stress can describe the experimental results very well.

We have clarified that the sequence of events in the bursting process, i.e. ejections, sweeps and interactions, bears a direct relation to the turbulent energy budget via the turbulent diffusion. We have noted that up to the middle of the equilibrium region the roughness effect is marked and sweeps may become more dominant than ejections with increasing roughness.

REFERENCES

ANTONIA, R. A. & ATKINSON, J. D. 1973 *J. Fluid Mech.* **58**, 581.

BRADSHAW, P. 1971 *An Introduction to Turbulence and its Measurement.* Pergamon.

BREMHORST, K. & WALKER, T. B. 1973 *J. Fluid Mech.* **61**, 173.

BRODKEY, R. S., WALLACE, J. M. & ECKELMANN, H. 1974 *J. Fluid Mech.* **63**, 209.

CORINO, E. R. & BRODKEY, R. S. 1969 *J. Fluid Mech.* **37**, 1.

ECKELMANN, H. 1974 *J. Fluid Mech.* **65**, 439.

FRENKIEL, F. N. & KLEBANOFF, P. S. 1967 *Phys. Fluids*, **10**, 507.

FRENKIEL, F. N. & KLEBANOFF, P. S. 1973 *Phys. Fluids*, **16**, 725.

GRASS, A. J. 1971 *J. Fluid Mech.* **50**, 233.

GUPTA, A. K. & KAPLAN, R. E. 1972 *Phys. Fluids*, **15**, 981.

HINO, M., SAWAMOTO, N. & TAKASU, S. 1975 *Proc. Japan Soc. Civil Engrs*, no. 237, p. 75 (in Japanese).

KAMPÉ DE FÉRIET, J. 1966 *David Taylor Model Basin Rep.* no. 2013.

KIM, H. T., KLINE, S. J. & REYNOLDS, W. C. 1971 *J. Fluid Mech.* **50**, 133.

KLINE, S. J., REYNOLDS, W. C., SCHRAUB, F. A. & RUNSTADLER, P. W. 1967 *J. Fluid Mech.* **30**, 741.

KOVASZNAY, L. S. G., KIBENS, V. & BLACKWELDER, R. F. 1970 *J. Fluid Mech.* **41**, 283.

LAUFER, J. 1954 *N.A.C.A. Tech. Rep.* TR-1174.

LAWN, C. J. 1971 *J. Fluid Mech.* **48**, 477.

LU, S. S. & WILLMARTH, W. W. 1973 *J. Fluid Mech.* **50**, 481.

MOLLO-CHRISTENSEN, E. 1971 *A.I.A.A. J.* **9**, 1217.

MONIN, A. S. & YAGLOM, A. M. 1971 *Statistical Fluid Mechanics*, vol. 1, p. 205. M.I.T. Press.

NAKAGAWA, H. & NEZU, I. 1974 *Proc. Japan Soc. Civil Engrs*, no. 231, p. 61.

NAKAGAWA, H., NEZU, I. & UEDA, H. 1975 *Proc. Japan Soc. Civil Engrs*, no. 241, p. 155.

NYCHAS, S. G., HERSHEY, H. C. & BRODKEY, R. S. 1973 *J. Fluid Mech*, **61**, 513.

OFFEN, G. R. & KLINE, S. J. 1974 *J. Fluid Mech.* **62**, 223.

ROTTA, J. C. 1972 *Turbulente Strömungen*. Teubner.

WALLACE, J. M., ECKELMANN, H. & BRODKEY, R. S. 1972 *J. Fluid Mech.* **54**, 39.

WILLMARTH, W. W. & LU, S. S. 1972 *J. Fluid Mech.* **55**, 65.

ZARIČ, Z. 1972 *Comptes Rendus*, A **269**, 513.